Supporting Information for "What is the neutral wind in height-integrated ionospheric electrodynamics?"

S. M. Hatch[1] *, J. K. Burchill[2], H. Vanhamäki[3], R. L. A. Mesquita[4], K. M. Laundal[1], D. J. Knudsen[2]

[1]Department of Physics and Technology, University of Bergen, Bergen, Norway

[2]Department of Physics and Astronomy, University of Calgary, Calgary, Alberta, Canada

[3]Space Physics and Astronomy Research Unit, University of Oulu, Oulu, Finland

[4]Johns Hopkins University Applied Physics Laboratory, Laurel, MD, USA

Contents of this file

Introduction

Text S1 describes how assuming the ionospheric electric field is independent of height in the presence of tilted field lines implicitly assumes that the electric field does not vary over scale sizes smaller than a predetermined limit. Text S2 provides a proof of the statement

———————

*Department of Physics and Technology,

University of Bergen, Bergen, Norway

May 1, 2024, 4:29am

in the main text that the following inequality is true: $\int \sigma_P |\mathbf{u} \times \mathbf{B}|^2 dh \geq \Sigma_P |\mathbf{U}_P \times \mathbf{B}|^2$. Text S3 summarizes the Ieda (2020) procedure for calculating Hall and Pedersen conductivity profiles.

Table S1 summarizes some details of each rocket, including the time of each measurement (center time of images used for triangulation of chemical release experiments) and the availability of Poker Flat Incoherent Scatter Radar (PFISR) measurements.

Figure S1 illustrates how conductivity profiles derived from PFISR measurements and empirical models are used together with neutral wind profiles derived from chemical release experiements to estimate the Hall- and Pedersen-weighted neutral winds.

Text S1: Relationship between assumed E-field height independence and scale size of variations

Suppose magnetic field lines are locally tilted by an angle θ relative to the vertical direction (i.e., inclination $I = 90° - \theta$), and that we have a coordinate system $x'yz'$ that is such that z' is parallel to field lines locally and x' and y are perpendicular. This coordinate system is tilted relative to a local xyz coordinate system, with the x direction of the latter determined by ensuring that the field lines are contained within the xz plane and the z direction upward. The transformations from xyz to $x'yz'$ coordinates are then

$$x' = x \cos \theta - z \sin \theta;$$

$$z' = x \sin \theta + z \cos \theta.$$

The perpendicular electric field $\mathbf{E}_\perp (x', y) = \mathbf{E}_\perp (x \cos \theta - z \sin \theta, y) = E_{\perp, x'} \hat{\mathbf{x}}' + E_{\perp, y} \hat{\mathbf{y}}$.

Averaging the electric field over height at $x = 0$, we find

$$\langle \mathbf{E}_\perp \rangle = \int_{z_1}^{z_2} \mathbf{E}_\perp (-z \sin \theta, y) dz / (z_2 - z_1), \tag{1}$$

If $\mathbf{E}_\perp$ is constant with altitude, it is equivalently constant over a horizontal distance $d = (z_2 - z_1) \sin \theta$. For example, if the local field inclination $I = 70°$ and the effective vertical extent of the ionosphere $\Delta_z = z_2 - z_1 = 50$ km, assuming $\mathbf{E}_\perp$ does not vary with altitude is equivalent to assuming that it does not vary within a circle of radius $d = 17$ km, or about $0.2°$. The situation is more drastic in the Southern Hemisphere, where if the inclination $I = 50°$ the radius of the circle is ~ 30 km, or $0.3°$. (As an example of where this could be taken into account, see text right after Equation 9 in Aikio et al. (2012).)

May 1, 2024, 4:29am

Text S2: Cauchy-Bunyakovsky-Schwarz proof

Let $L^2_w(X, \mu)$ be a weighted L^2 space over X with measure μ. The corresponding inner product for functions f and g is

$$\langle f, g \rangle = \int_X f(t)\overline{g(t)}w(t)dt, \tag{2}$$

with $w(t) > 0$ for all t. The inner product (2) obeys the Cauchy-Bunyakovsky-Schwarz inequality

$$|\langle f, g \rangle|^2 \leq \langle f, f \rangle \langle g, g \rangle.$$

Taking $f = 1$, $g = u_i$ (the ith component of the neutral wind $\mathbf{u}$), and $\mu = \sigma_P$, we have

$$\left| \int \sigma_P u_i dh \right|^2 = \Sigma_P^2 U_{P,i}^2 \leq \Sigma_P \int \sigma_P u_i^2 dh,$$

or rearranging,

$$\int \sigma_P u_i^2 dh \geq \Sigma_P U_{P,i}^2.$$

Summing this inequality for each component of $\mathbf{u}$ we find

$$\int \sigma_P |\mathbf{u}|^2 dh \geq \Sigma_P |\mathbf{U}_P|^2. \tag{3}$$

If in addition the magnetic field $\mathbf{B}$ is approximately constant between altitudes of $\sim$80–200 km, then multiplying both sides of Inequality 3 by $|\mathbf{B}\sin\theta|^2$ and applying the geometric definition of the cross product ($|\mathbf{u}||\mathbf{B}|\sin\theta = \mathbf{u} \times \mathbf{B}$) we have

$$\int \sigma_P |\mathbf{u} \times \mathbf{B}|^2 dh \geq \Sigma_P |\mathbf{U}_P \times \mathbf{B}|^2. \tag{4}$$

Text S3: Calculation of conductivity profiles

Hall and Pedersen conductivity profiles σ_H and σ_P are derived following Ieda (2020), with

$$(\sigma_H,\, \sigma_P) = (\sigma_{H,e} - \sigma_{H,i},\, \sigma_{P,e} + \sigma_{P,i}). \tag{5}$$

Subscripts e and i refer to the contributions from electrons and ions. For each conductivity the ion contribution is a sum over ion species:

$$\sigma_{\{H,P\},i} = \sum_{l=\mathrm{NO^+,O_2^+,O^+}} \sigma_{\{H,P\},l}. \tag{6}$$

The contribution from each charged particle species j ($\mathrm{NO^+}$, $\mathrm{O_2^+}$, $\mathrm{O^+}$, and e^-) is given by

$$(\sigma_{H,j},\, \sigma_{P,j}) = \frac{en_j}{B}\left(\frac{k_j^2}{1+k_j^2},\, \frac{k_j}{1+k_j^2}\right), \tag{7}$$

with $k_j = \Omega_j/\nu_{jn}$, and Ω_j and ν_{jn} respectively the gyrofrequency and collision frequency for momentum transfer between charged particle species j and neutrals.

Expressions for ν_{jn} are given in Appendix A of Ieda (2020) for the three ion species just mentioned and neutral species N_2, O_2, and O. These expressions take stock of non-resonant collisions between parental pairs such as O_2^+ and O_2 that are neglected by, for example, Schunk & Nagy (2009), but are nevertheless an essential part of the description of ion-neutral collisions for ion and neutral temperatures below approximately 600 K.

Figure S1 illustrates the quantities involved in the calculation of conductivity for a wind profile measured during the Mesospheric Inversion Layer Stratified Turbulence (MIST) campaign on January 26, 2015. In Figure S1a densities of neutral species are given by the NRLMSIS®2.0 empirical atmospheric model (Emmert et al., 2020). In Figure S1b the electron density (labeled e^-) is measured by PFISR, and the ion species densities are given by multiplying the electron density by the fractional composition of each species as

given by the International Reference Ionosphere (IRI) 2016 model (Bilitza et al., 2017). In Figure S1c the electron and ion temperatures are measured by PFISR, and the neutral temperature is given by IRI 2016.

From these density and temperature profiles we calculate collision frequencies (Figure S1d) and conductivity profiles (Figure S1e) that are ultimately used to estimate the zonal (labeled U_H and U_P) and meridional (labeled V_H and V_P) components of the Hall- and Pedersen-weighted neutral winds, which are indicated with vertical lines in Figure S1f.

Table S1. Rockets from which neutral wind measurements are used in this study.

Rocket	Date	Launch [UT]	Alt range [km]	PFISR alt range[a,b] [km]	PFISR meas. [UT]	Reference
Joule II	2007-01-19	12:31	93.5–140.0	91–300	12:30:00	Burchill et al. (2012)
		12:47	91–140	91–274	12:45:20	Sangalli et al. (2009)
		12:48	92–128.5	91–274	12:45:20	
HEX II	2007-02-14	09:36	91–150	91–326	09:46:08	Scott (2009)
		09:38	95–152	91–326	09:46:08	
MIST	2015-01-26	09:15	90–144		09:14:55	Larsen et al. (2022)
		09:19	86–150		09:19:56	
		09:48	90–148	83–345	09:44:55	
		09:52	88–152		09:49:56	
Auroral	2017-03-02	05:44	102–187		05:44:11	
Jets		05:47	98–183		05:47:15	Akbari et al. (2022)
Super	2018-01-26	14:12	82–320		14:03:36	Mesquita et al. (2020)
Soaker		14:16	96–153	88–320	14:18:41	
		14:49	81–157	85–347	14:48:51	
		14:52	86–145	85–347	14:48:51	

[a]We exclude PFISR measurements for which $\sigma_{n_e}/n_e \geq 1$. (n_e: plasma density. σ_{n_e}: plasma density uncertainty.)

[b]Valid PFISR measurements available over 87–345 km unless otherwise noted.

References

Aikio, A. T., Cai, L., & Nygrén, T. (2012, oct). Statistical distribution of height-integrated energy exchange rates in the ionosphere. *Journal of Geophysical Research: Space Physics*, *117*(A10). Retrieved from `https://doi.org/10.1029/2012JA018078` doi: 10.1029/2012JA018078

Akbari, H., Pfaff, R., Clemmons, J., Freudenreich, H., Rowland, D., & Streltsov, A. (2022, 2). Resonant alfvén waves in the lower auroral ionosphere: Evidence for the nonlinear evolution
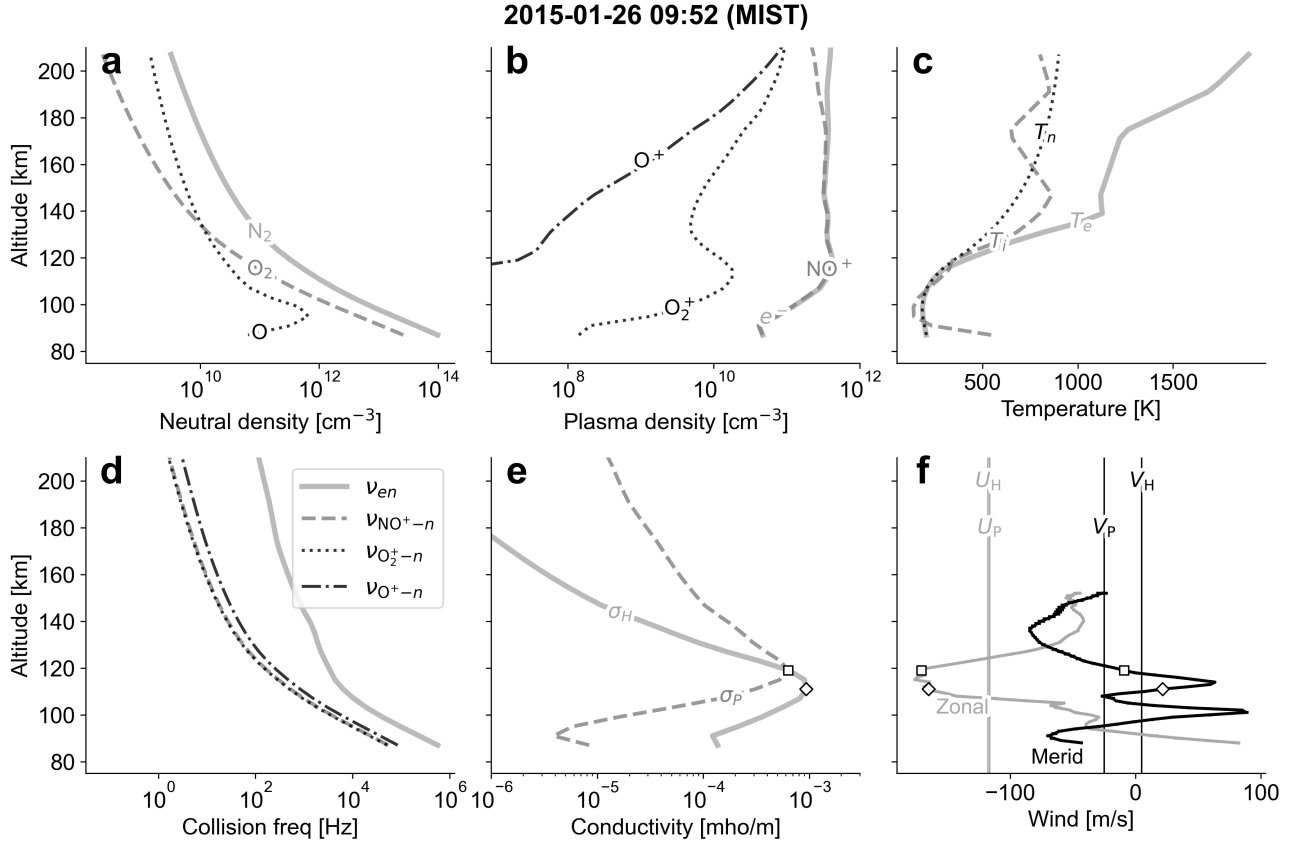
2015-01-26 09:52 (MIST)

Figure S1. Illustration of altitude profiles needed for calculation of zonal and meridional components of the Hall- and Pedersen-weighted winds via Equation 10 in the main text. These profiles correspond to the MIST rocket launched 2015-01-26 09:52 UT during moderate geomagnetic activity ($K_p = 4.0$; see Figure 1c1–c3 in the main text). (a) Neutral density profiles from NRLMSIS®2.0 model. (b) PFISR plasma density profile (e^-) with fractional ion species densities given by IRI 2016. (c) PFISR electron and ion temperature profiles, and IRI 2016 neutral temperature profile. (d) Ion-neutral collision frequencies calculated from profiles in panels a–c. (e) Hall and Pedersen conductivity profiles (solid and dashed lines). The peaks of the Hall and Pedersen conductivity profiles are respectively indicated by a diamond and a square. (f) Neutral wind profiles. Zonal (U_H and U_P) and meridional (V_H and V_P) components of the Hall- and Pedersen-weighted neutral winds are indicated with vertical lines. Neutral wind components at peaks of the Hall and Pedersen conductivity profiles respectively also indicated by diamond and square symbols.

May 1, 2024, 4:29am

of the ionospheric feedback instability. *Journal of Geophysical Research: Space Physics*, *127*. doi: 10.1029/2021JA029854

Bilitza, D., Altadill, D., Truhlik, V., Shubin, V., Galkin, I., Reinisch, B., & Huang, X. (2017, 2). International reference ionosphere 2016: From ionospheric climate to real-time weather predictions. *Space Weather*, *15*, 418-429. doi: 10.1002/2016SW001593

Burchill, J. K., Clemmons, J. H., Knudsen, D. J., Larsen, M., Nicolls, M. J., Pfaff, R. F., . . . Sangalli, L. (2012, 2). High-latitude e region ionosphere-thermosphere coupling: A comparative study using in situ and incoherent scatter radar observations. *Journal of Geophysical Research: Space Physics*, *117*. doi: 10.1029/2011JA017175

Emmert, J. T., Drob, D. P., Picone, J. M., Siskind, D. E., Jones, M., Mlynczak, M. G., . . . Yuan, T. (2020, sep). NRLMSIS 2.0: A whole-atmosphere empirical model of temperature and neutral species densities. *Earth and Space Science*. Retrieved from `https://onlinelibrary.wiley.com/doi/10.1029/2020EA001321` doi: 10.1029/2020EA001321

Ieda, A. (2020, feb). Ion-Neutral Collision Frequencies for Calculating Ionospheric Conductivity. *Journal of Geophysical Research: Space Physics*, *125*(2). Retrieved from `https://onlinelibrary.wiley.com/doi/10.1029/2019JA027128` doi: 10.1029/2019JA027128

Larsen, M. F., Pfaff, R. F., Mesquita, R., & Kaeppler, S. R. (2022, 1). Gradient winds and neutral flow dawn-dusk asymmetry in the auroral oval during geomagnetically disturbed conditions. *Journal of Geophysical Research: Space Physics*, *127*. Retrieved from `https://onlinelibrary.wiley.com/doi/10.1029/2021JA029936` doi: 10.1029/2021JA029936

Mesquita, R. L. A., Larsen, M. F., Azeem, I., Stevens, M. H., Williams, B. P., Collins, R. L., & Li, J. (2020, 8). In situ observations of neutral shear instability in the statically stable high-latitude mesosphere and lower thermosphere during quiet geomagnetic conditions. *Journal of*

Geophysical Research: Space Physics, *125*. doi: 10.1029/2020JA027972

Sangalli, L., Knudsen, D. J., Larsen, M. F., Zhan, T., Pfaff, R. F., & Rowland, D. (2009, apr). Rocket-based measurements of ion velocity, neutral wind, and electric field in the collisional transition region of the auroral ionosphere. *Journal of Geophysical Research: Space Physics*, *114*(A4). Retrieved from `http://doi.wiley.com/10.1029/2008JA013757` doi: 10.1029/2008JA013757

Schunk, R., & Nagy, A. (2009). *Ionospheres* (Second ed.). Cambridge: Cambridge University Press. Retrieved from `http://ebooks.cambridge.org/ref/id/CBO9780511635342` doi: 10.1017/CBO9780511635342

Scott, T. (2009). Analysis of the neutral wind profiles from the hex ii experiment.